JOC The Journal of Organic Chemistry

Article

pubs.acs.org/joc

Soluble Diazaiptycenes: Materials for Solution-Processed Organic Electronics

Philipp Biegger,[†] Sebastian Stolz,[‡,§] Sebastian N. Intorp,[†] Yexiang Zhang,[⊥,#] Jens U. Engelhart,[†] Frank Rominger,[†] Kenneth I. Hardcastle,[▽] Uli Lemmer,[§,∥] Xuhong Qian,[#] Manuel Hamburger,[†,‡] and U. H. F. Bunz*[,†,○]

[†]Organisch-Chemisches Institut, Ruprecht-Karls-Universität Heidelberg, Im Neuenheimer Feld 270, 69120 Heidelberg, Germany

[‡]InnovationLab GmbH, Speyerer Straße 4, 69115 Heidelberg, Germany

[§]Lichttechnisches Institut, Karlsruher Institut für Technologie, Engesser Straße 13, 76131 Karlsruhe, Germany

[∥]Institute of Microstructure Technology, Karlsruhe Institute of Technology, Hermann-von-Helmholtz-Platz 1, 76344 Eggenstein-Leopoldshafen, Germany

[⊥]School of Chemistry and Biochemistry, Georgia Institute of Technology, 901 Atlantic Drive, Atlanta, Georgia 30332, United States

[#]Shanghai Key Laboratory of Chemical Biology, State Key Laboratory of Bioreactor Engineering, School of Pharmacy, East China University of Science and Technology, Shanghai 200237, People's Republic of China

[▽]Department of Chemistry, Emory University, 1515 Dickey Drive, Atlanta, Georgia 30322, United States

[○]Centre for Advanced Materials, Ruprecht-Karls-Universität Heidelberg, Im Neuenheimer Feld 225, 69120 Heidelberg, Germany

Supporting Information

ABSTRACT: The synthesis and characterization of soluble azaiptycenes is reported. Optical and physical properties were studied and compared with those of the structurally consanguine azaacenes. Electrochemical experiments and quantum-chemical calculations revealed the electronic structure of the iptycene derivatives. Their crystallization behavior was examined. A highly fluorescent amorphous diazatetracene derivative was integrated into a simple organic light-emitting diode, showing enhanced performance compared with that of previously reported, structurally similar tetracenes.

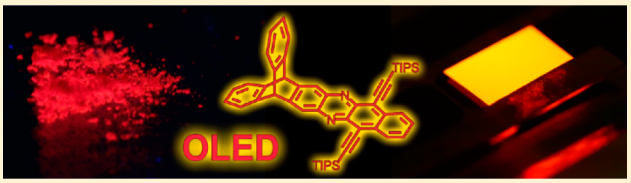

INTRODUCTION

We herein describe the synthesis of an amorphous iptycene-appended diazatetracene and demonstrate its usefulness as emitter layer in an organic light-emitting diode (OLED). In general, the larger acenes have impacted the field of organic electronics. When equipped with silylethynyl groups, tetracene and pentacene become stable and processable yet retain their crystallinity.[1,2] High charge mobility with applications in thin-film transistors is the field of focus for acenes. However, higher-substituted acenes are also useful as emitting layers (EMLs) in light-emitting diodes, as shown by Anthony and co-workers.[3] Tetracenes **A** and **B** were used in substance, while pentacene **C** was employed in an Alq_3 matrix as a dopant[4] (Chart 1). **C** is a competitive red emitter. The seminal paper on tetracenes **A** and **B** describes their emission as red or red-orange. Although **A** and **B** are crystalline, they showed surprisingly narrow emission peaks in their solid-state photoluminescence (PL). Their use as EMLs in OLEDs, while successful, gave devices with luminances of 1 cd/m^2 (**A**, 12 V) and 5 cd/m^2 (**B**, 18 V). These OLEDs were not bright. Intermolecular deactivation, nonradiative energy loss, and excimer formation are enhanced through the efficient packing of crystalline **A** and **B**. Also, electron injection is probably not facile in either **A** or **B**.

Chart 1. Examples of Acenes Reported as OLED Emitters

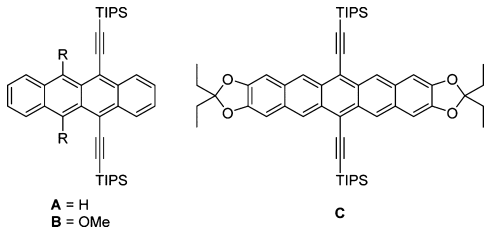

Nevertheless, this report spurred us to ask whether tetracene derivatives could be made more competitive by molecular engineering. Electron injection should be improved by lowering the LUMO through the introduction of nitrogen atoms into the aromatic system.[5] The addition of an iptycene unit should modify the packing to disrupt unwanted energy transfer in the excited state and isolate the tetracene fluorophore.[6−9] The concept of utilizing iptycene in emissive molecules or as host materials in electroluminescent devices has been used

Received: November 10, 2014
Published: November 19, 2014

ACS Publications © 2014 American Chemical Society

Scheme 1. Synthesis of Triptycene-Based *N*-Heteroacenes 1a−3a: While 1a Was Synthesized via Classical Condensation Route (Method a),[14] 2a and 3a Could Also Be Synthesized through Buchwald−Hartwig Coupling (Method b)[15]

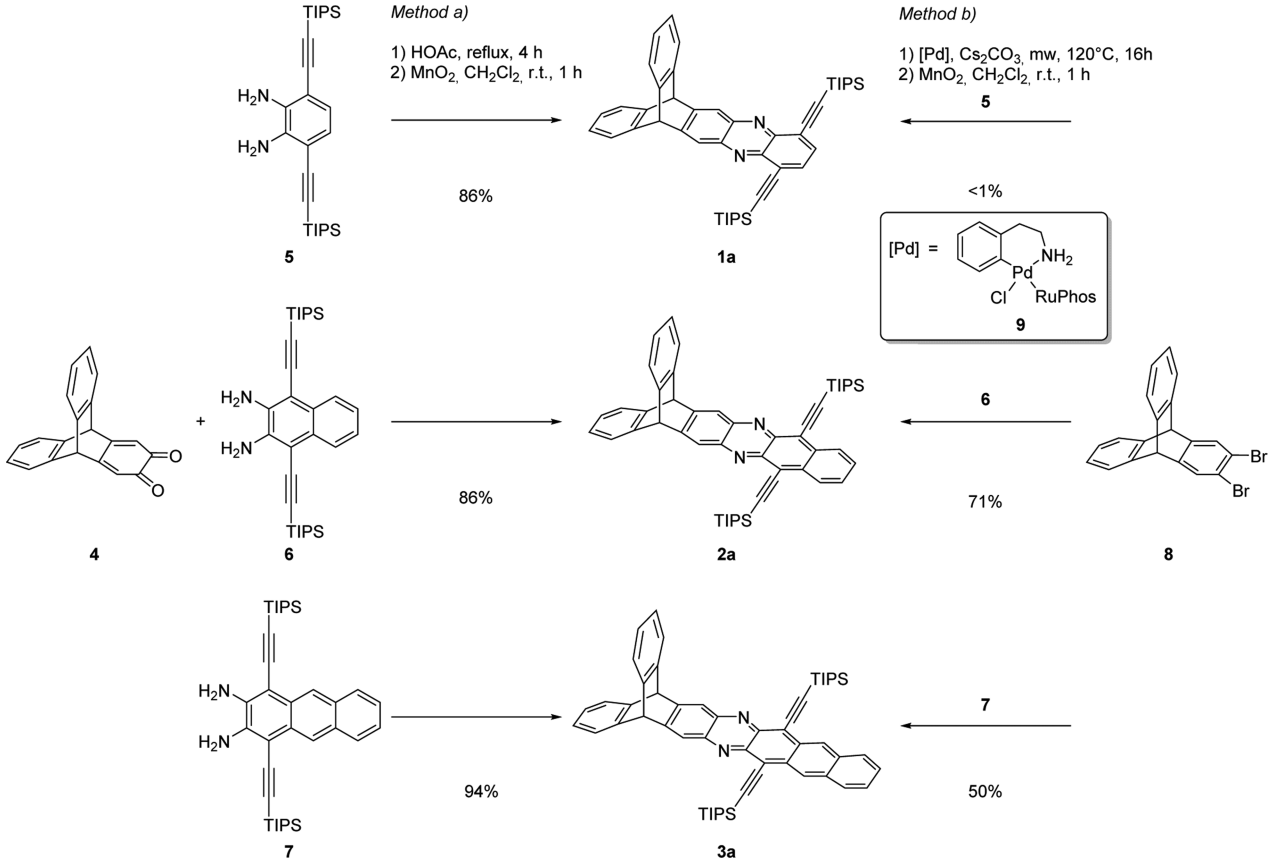

successfully.[10−13] However, the combination of heteroacenes with triptycene has not been reported. The attached TIPS-ethynyl units give solution-processable materials for organic optoelectronics. Here we present the synthesis of diazaiptycenes and the application of a diazatetracene in proof-of-concept OLEDs.

RESULTS AND DISCUSSION

Synthesis. The synthesis of TIPS-ethynylated diazaiptycenes is shown in Scheme 1. The higher azaacenes **2a** and **3a** were synthesized in good to excellent yields via ring-closing Buchwald−Hartwig cross-coupling reactions of 2,3-dibromotriptycene (**8**) and the diaminoacenes **6** and **7**, respectively, under optimized microwave conditions.[15] Direct oxidation of the intermediates with manganese dioxide led to the target molecules **2a** and **3a**. The phenazine derivative **1a** was formed only in traces using Buchwald−Hartwig coupling, but condensation of triptycene-2,3-quinone (**4**) with **6** gave **1a** in 86% yield. We also applied the condensation method for the synthesis of **2a** and **3a**, improving the yields to 86% and 94%, respectively. The exceptional stability of *o*-quinone **4** is advantageous. The diazatetracenes and -pentacenes can be formed by Buchwald−Hartwig coupling and also by condensation. All of the diazaiptycenes were well-soluble in polar and nonpolar organic solvents and air-stable as solids for extended periods of time. In acidic media, the reduced *N*,*N*′-dihydro compounds form. To investigate the influence of the triptycene moiety on the azaacenes, we compared the properties of **1a−3a** to those of the previously reported[14,16,17] heteroacenes **1b−3b** (Chart 2).

Chart 2. Phenazine 1b,[14] Diazatetracene 2b,[16] and Diazapentacene 3b[17]

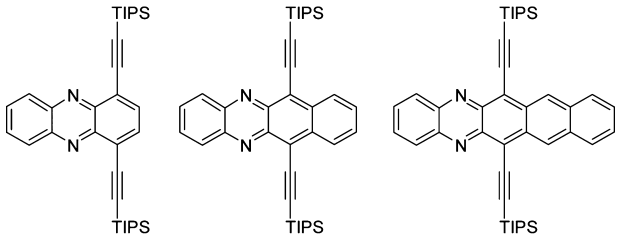

Optical Properties. **1a−3a** exhibit bright colors in the solid state (Figure 1). While **1a** appears yellow with a yellow fluorescence, diazatetracene **2a** is deep-red with strong orange to light-red fluorescence. **3a** has a dark-green color but is nonfluorescent in the solid state. This trend is observed in solutions, where **2a** exhibits a deep color in daylight and strong yellow-orange emission under illumination at 365 nm, while **1a** and **3a** are less strongly fluorescent (Figure 1).

Figure 2a shows the absorption spectra of compounds **1a−3a** compared with those of the *N*-heteroacenes **1b−3b**[14,17,18] in hexane. The diazaiptycenes showed curves similar to those of the diazaacenes, indicating that there is no significant electronic coupling between the two isolated benzene rings and the azaacene unit. All exhibited the characteristic fine structure of acenes in the long-wavelength range, with the longest-wavelength absorptions for **1a−3a** at 435, 558, and 675 nm being blue-shifted compared with the bands in the unsub-

dx.doi.org/10.1021/jo502564w | J. Org. Chem. 2015, 80, 582−589

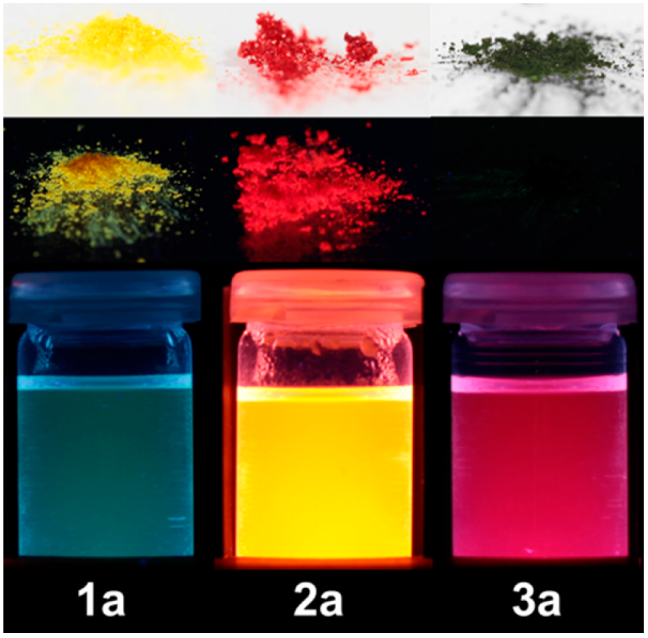

Figure 1. Photographs of solid **1a**, **2a**, and **3a** in daylight (top) and under black light with illumination at 365-nm (middle) and of **1a**, **2a**, and **3a** in hexane solution under black light with illumination at 365 nm (bottom).

stituted acenes. The absorption maxima for **1a**–**3a** are blue-shifted by 5, 12, and 18 nm relative to those of the corresponding unsubstituted azaacenes (Table 1). The reason for the blue shift is probably the change in hybridization of the aromatic carbon atoms that attach the dihydroanthracene unit to the azaacene, which destabilizes the LUMO somewhat more than the HOMO. The emission spectra of **1**–**3** in solution reveal the same tendency (Figure 2b). The hypsochromic shifts for the diazaiptycenes were measured to be 8 nm for **1a**, 9 nm for **2a**, and 17 nm for **3a**. **2a** exhibits strong fluorescence with Φ = 57% in hexane and Φ = 76% in dichloromethane. **1a** is less fluorescent with Φ = 2% in hexane and dichloromethane, and **3a** displays Φ = 45% in hexane and Φ = 11% in dichloromethane. The excited state of **2a** is long-lived with τ = 18.3 ns, whereas **1a** showed two emission lifetimes (Table 1).

Electrochemistry and Quantum-Chemical Calculations. To approximate the ionization potentials and electron affinities, we performed cyclic voltammetry (CV) measurements with ferrocene as the internal reference. **1a**–**3a** display one pseudoreversible reduction peak $E^{(0/-)}$ and no oxidation peak (Table 2; also see the Supporting Information). For **1a**–**3a** the potentials are −1.72, −1.34, and −1.19 V, respectively, allowing the LUMO levels to be estimated as −3.36, −3.75, and −3.92 eV. From these LUMO values and the optical gaps, the HOMO energies were calculated to be −6.10 eV for **1a**, −5.91 eV for **2a**, and −5.71 eV for **3a**. **2a** and **3a** exhibit a second reduction peak $E^{(-/2-)}$, while the potential for **1a** is probably out of the stability window of the respective solvent system. Further examination of the effect of the iptycene on the diazaacenes was conducted through DFT calculations (B3LYP/6-311++G**).[20]

The shapes of the frontier molecular orbitals (FMOs) of **1a**–**3a** are similar to those of the equivalent azaacenes **1b**–**3b** (e.g., those for **2a** and **2b** are shown in Figure 3; for **1a**/**1b** and **3a**/**3b**, see the Supporting Information). Both the HOMO and LUMO are located on the azaacene moiety and do not leach into the triptycenyl unit. The calculated absolute energy levels differ by up to 0.56 eV from those derived from experimental data (Table 2) but are in good agreement with the experimental findings of blue-shifted absorption spectra for the diazaiptycenes due to an increased optical band gap relative to that of the acenes **1b**–**3b**. This increase results from a stronger destabilizing effect of the substituent on the LUMO because of its higher coefficient at the two substituted carbon atoms,[22] probably as an effect of homoconjugation and possibly of changed hybridization. The FMO calculations confirmed the lack of *direct* conjugation over the methine bridges of the triptycene. We correlated the calculated LUMO values with the first reduction potentials measured by CV according to Bunz *et al.* (see the Supporting Information). The values fit properly

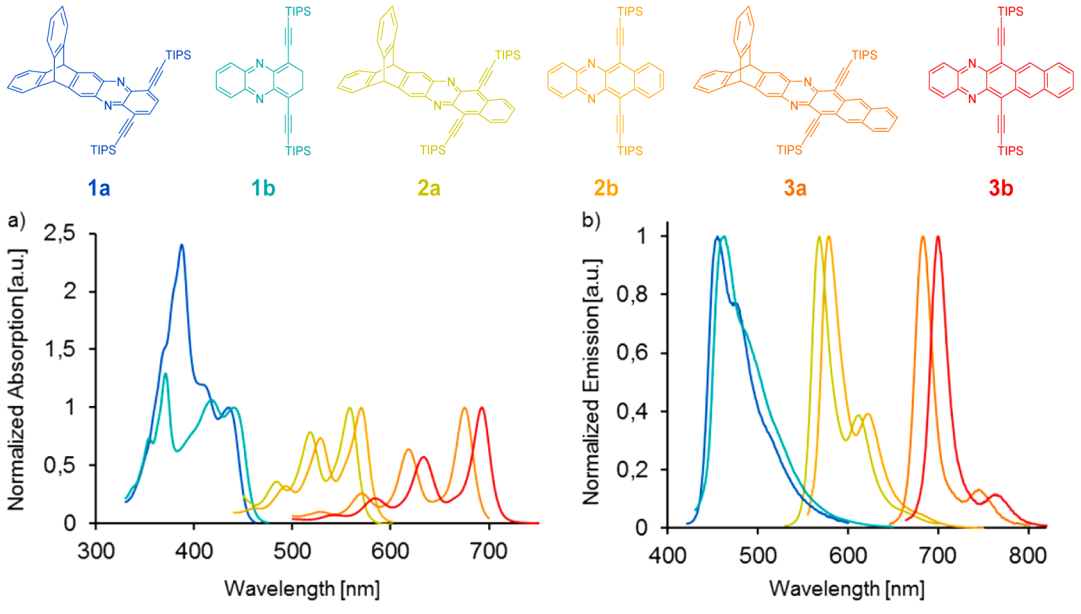

Figure 2. (a) Long-wavelength normalized UV–vis absorption spectra and (b) normalized emission spectra of **1a**–**3b** in hexane.

dx.doi.org/10.1021/jo502564w | *J. Org. Chem.* 2015, 80, 582–589

Table 1. Photophysical Properties of 1a−3b in Solution[a]

	in hexane						in dichloromethane				
compd	λ_{max}^{abs} [nm]	λ_{edge}^{abs} [nm]	λ_{max}^{em} [nm]	Stokes shift [nm]	Φ	τ [ns]	λ_{max}^{abs} [nm]	λ_{max}^{em} [nm]	Stokes shift [nm]	Φ	τ [ns]
1a	435	453	455	20	0.02	0.10/3.10	435	473	38	0.02	0.24/3.40
1b	440	460	463	23	–	–	439	492	53	0.02[b]	0.37[b]
2a	558	574	568	10	0.57	13.3	562	593	31	0.76	18.3
2b	570	585	577	7	–	–	570	609	39	–	–
3a	675	692	682	7	0.45	15.6	683	718	35	0.11	7.8
3b	693	709	699	6	<0.01[c]	–	697	738	41	–	–

[a]Optical spectroscopy absorption maxima (λ_{max}^{abs}), absorption edges (λ_{edge}^{abs}), emission maxima (λ_{max}^{em}), Stokes shifts, quantum yields (Φ), and lifetimes (τ) are shown. [b]Taken from ref 14. [c]Taken from ref 17.

Table 2. Experimental and Calculated (Gas-Phase) Properties of 1a−3b

compd	$E^{(0/-)}$ [V][a]	E_{HOMO} [eV][b]	E_{LUMO}^{CV} [eV][c]	E_{gap}^{UV} [eV][d]	E_{HOMO}^{DFT} [eV][e]	E_{LUMO}^{DFT} [eV][e]	E_{g}^{DFT} [eV][e]
1a	−1.72	−6.10	−3.36	2.74	−5.87	−2.93	2.94
1b	−1.68	−6.12	−3.42	2.70	−5.97	−3.08	2.88
2a	−1.34	−5.91	−3.75	2.16	−5.45	−3.20	2.25
2b	−1.23[f]	−5.99	−3.87	2.12	−5.54	−3.35	2.20
3a	−1.19	−5.71	−3.92	1.79	−5.16	−3.36	1.80
3b	−1.05[g]	−5.80	−4.05	1.75	−5.25	−3.50	1.75

[a]First reduction potentials measured by cyclic voltammetry (CV) in tetrahydrofuran with Bu_4NPF_6 as the electrolyte against Fc/Fc^+ as an internal standard (−5.10 eV)[19] at 0.2 mV/s. [b]$E_{HOMO} = E_{LUMO}^{CV} - E_{gap}^{UV}$. [c]Calculated from CV measurements ($E_{LUMO}^{CV} = -5.10\ eV - E^{(0/-)}$). [d]Calculated from λ_{edge}^{abs} in hexane. [e]Obtained from quantum-chemical calculations with TURBOMOLE B3LYP/def2-TZVP//Gaussian09 B3LYP/6-311++G**.[20,21] [f]Taken from ref 16. [g]Taken from ref 17.

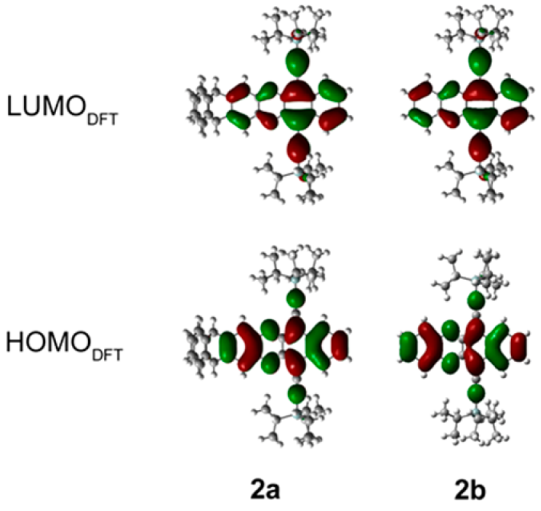

Figure 3. Quantum-chemical calculations (TURBOMOLE B3LYP/def2-TZVP//Gaussian09 B3LYP/6-311++G**)[20,21] of the FMOs for compounds **2a** and **2b**.

into the correlation plot, indicating a small reorganization energy of the heteroiptycenes.[23,24]

Solid-State Structure. The solid-state structure is an important factor for the usefulness of compounds as organic semiconductors in electronic devices. However, among the diazaiptycenes we could only obtain crystals for **1a** (dark-yellow needles). The presence of guest solvent molecules indicates a packing with some void space. However, the crystal exhibits a density of about 1 g/cm^3. Figure 4 depicts the arrangement of **1a** in the solid. The phenazine forms a dimer structure rotated

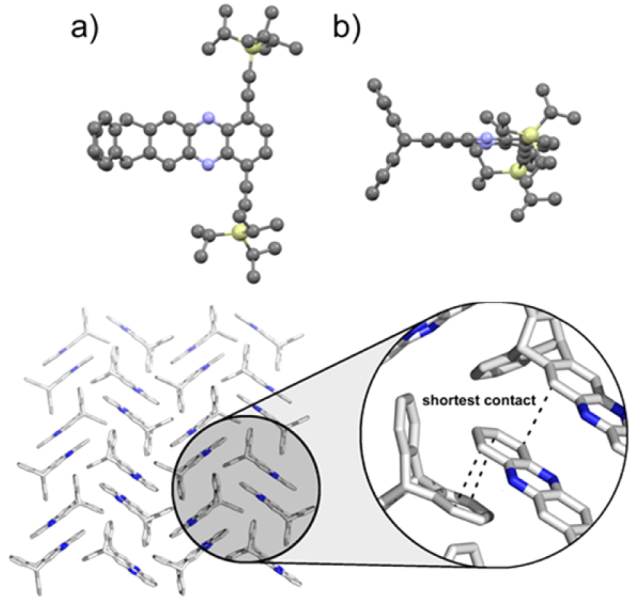

Figure 4. Top: (a) top view and (b) side view of the crystal structure of **1a** (solvent molecules and hydrogen atoms omitted for clarity). Bottom: crystal packing of **1a** (TIPS-ethynyl side chains hidden for clarity).

by 180° with the pyrazine rings directly on top of each other and the adjacent molecules laterally displaced. Hence, the acene backbones show little joint overlap, attributed to the bulky TIPS substituents. In the second dimension, the molecule shows a one-dimensional array; the outer benzene ring of the phenazine overlaps with one of the isolated benzene rings of the adjacent molecule. The molecular axes are slightly distorted against one another, giving a zigzag motif. There should be no significant electronic interaction throughout the crystal beyond the dimer. The packing is different from that of its related triptycenyl phenazine without the TIPS-ethynyl substituents (reported by Chong and MacLachlan[9]). The latter exhibits an interdigitated cofacial arrangement within one-dimensional stacks interlocked with one another, resulting in a two-dimensional layer.

We obtained crystals for **1b**, proving that the triptycenyl moiety is responsible for the longitudinal shift of the packing of the phenazine molecules relative to one another, as **1b** packs with the pyrazine ring on top of the adjacent benzene ring of the next phenazine molecule (Figure 5). For compounds **2a** and **3a**, specimens suitable for analysis could not be obtained, as amorphous powders resulted. The strongly emitting diazatetracene **2a** was employed as emitter for an OLED.

dx.doi.org/10.1021/jo502564w | J. Org. Chem. 2015, 80, 582−589

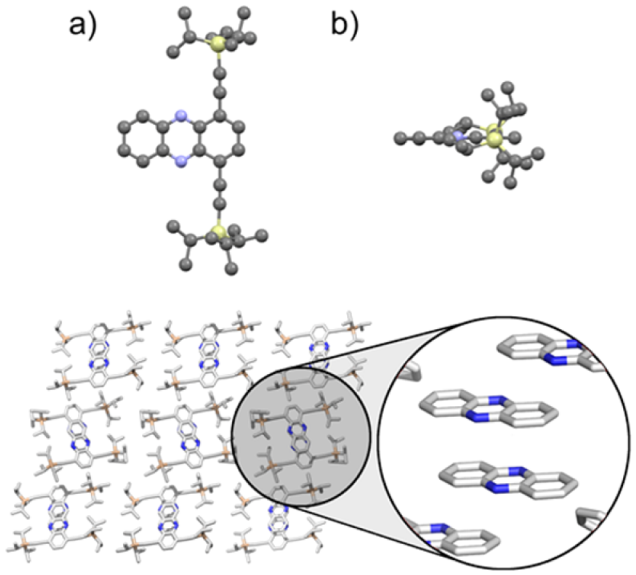

Figure 5. Top: (a) top view and (b) side view of the crystal structure of **1b** (hydrogen atoms omitted for clarity). Bottom: crystal packing of **1b** (right: TIPS-ethynyl side chains hidden for clarity).

Thin Films and OLED Fabrication of 2a. Amorphous powders should be promising OLED emitters, as nonradiative energy loss in OLED devices should be excluded.[25] While being amorphous is neither a sufficient nor necessary prerequisite for solid-state fluorescence, it can improve emissive quantum yields significantly, as shown here. We prepared thin films of **2a** to record photoluminescence spectra (for details, see the Supporting Information). **2a** is amorphous in thin films according to polarization microscopy and exhibits bright red-orange emission under illumination at 365 nm. The absorption and emission spectra of films of **2a** show a slight bathochromic shift and broadened peaks compared with solution spectra. A decrease in fine structure is a sign of aggregation in the solid state (Figure 6). The emission spectrum of films of **2a** (λ_{max}^{em} = 590 nm) is red-shifted by 22 nm compared with the emission in solution (λ_{max}^{em} = 568 nm). The quantum yield for **2a** in the film is lower than that in solution (Table 3). On the other hand, the highly crystalline diazaacene **2b** is not fluorescent in the solid state and is therefore useless as an emissive layer in OLEDs.[16] Attaching a triptycene to an acene core disrupts aggregation and thus allows the fluorescence in the solid state. Interestingly enough, the crystalline iptycene derivative **1a** is qualitatively much less solid-state-fluorescent than **2a**, while the larger derivative **3a** is nonfluorescent in the solid state. Consequently, we did not investigate the electroluminescence behavior of either **1a** or **3a**.

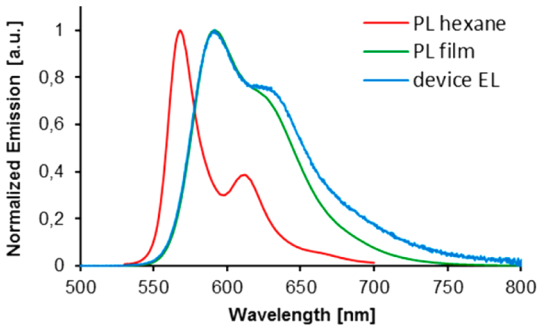

Figure 6. Photoluminescence emission spectra of **2a** in hexane (red) and in a thin film on a glass substrate (green) and electroluminescence spectrum of **2a** in an OLED device (blue).

Table 3. Photophysical Properties of Compound 2a in Hexane, in a Thin Film on a Glass Substrate, and in an OLED Device

	λ_{max}^{abs} [nm]	λ_{edge}^{abs} [nm]	λ_{max}^{em} [nm]	Stokes shift [nm]	Φ	E_{gap}^{UV} [eV][a]
PL in hexane	558	574	568	10	0.57	2.16
PL in film[b]	566	598	590	24	0.15	2.07
device EL[c]	n.a.	n.a.	591	n.a.	n.a.	n.a.

[a]Calculated from λ_{edge}^{abs}. [b]Spin-coated from toluene solution onto a glass substrate. [c]Data from an OLED device (see Figure 7).

We incorporated a solution-processed EML of **2a** in a simple OLED stack (Figure 7). A 60 nm thick layer of **2a** was spin-coated from toluene onto glass substrates covered by a 160 nm layer of indium tin oxide (ITO) and a 30 nm layer of poly(3,4-ethylenedioxythiophene):polystyrenesulfonate (PEDOT:PSS). As the cathode, a 10 nm layer of calcium followed by a 100 nm layer of aluminum was evaporated. The electroluminescence (EL) spectrum of this OLED is shown in Figure 6. The EL spectrum is similar to the thin-film photoluminescence spectrum but is slightly broadened (Table 3). In Figure 8,

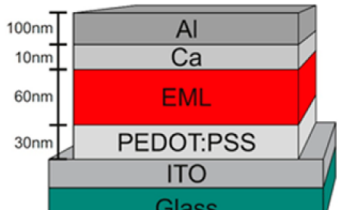

Figure 7. OLED device architecture with **2a** as the emission layer (EML).

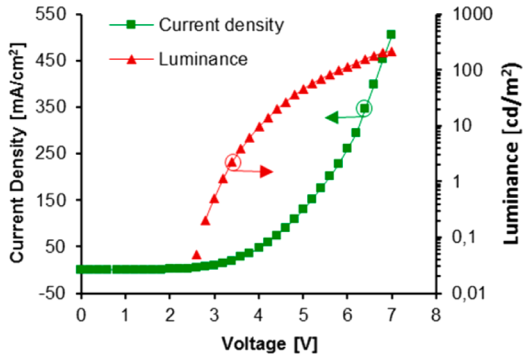

Figure 8. Luminance–voltage (red) and current density–voltage (green) plots of an OLED with **2a** as the emitter.

luminance–voltage and current density–voltage characteristics are shown. The OLED exhibits diodelike current density–voltage characteristics with a turn-on voltage of ~3 V. At 7 V, a luminance of >200 cd/m^2 is reached. In comparison with TIPS-tetracene **A**, **2a** shows significantly improved OLED performance, as **A** exhibited a turn-on voltage of ~5 V and a luminance of ~1 cd/m^2 at 12 V. The increase in device performance is a consequence of the molecular design of the emitter: the

dx.doi.org/10.1021/jo502564w | J. Org. Chem. 2015, 80, 582–589

triptycene unit suppresses aggregation, and the pyrazine facilitates balanced charge injection. These results demonstrate that triptycene combined with bulky substituents reduces aggregation in thin films while allowing sufficient charge transport and recombination for working OLED devices. Conceptually, this structural modification can easily be adapted to almost *any* other chromophore, suggesting that one can strengthen emissive qualities by the addition of triptycene units.[26]

CONCLUSION AND OUTLOOK

We synthesized stable and well-soluble azaacene-derived triptycenes **1a**−**3a**. *o*-Quinone condensation but also Buchwald−Hartwig coupling with *o*-diamines were successful. The targets **1a**−**3a** exhibit different solid-state structures, ranging from crystalline **1a** to amorphous solids **2a** and **3a**, depending on the length of the acene backbone and the position of the TIPS-ethynyl substituents. The amorphous and luminescent diazatetracene derivative **2a** was incorporated into a proof-of-concept OLED, showing improved device performance compared to the previously reported, structurally similar tetracenes **A** and **B**.[3] Further investigations of potential applications for the synthesized iptycenes are underway, together with the design of new azaiptycene derivatives.

EXPERIMENTAL SECTION

Materials and Methods. For microwave reactions, a Monowave 300 reactor from Anton Paar with an external IR temperature sensor was used. The palladium precatalyst RuPhos was purchased from Sigma-Aldrich with a purity of 95%. Thin-layer chromatography (TLC) was carried out on Polygram SIL G/UV$_{254}$ plates from Macherey, Nagel & Co. KG (Düren, Germany) and examined under ultraviolet irradiation (254 and 365 nm). Column chromatography was performed using silica gel from Macherey, Nagel & Co. (particle size: 0.032−0.062 mm). NMR spectra (^{1}H, ^{13}C) were recorded at room temperature at 400 MHz. Chemical shifts (δ) are given in parts per million (ppm) relative to internal solvent signals.[27] The following abbreviations describe the signal multiplicities: s = singlet, m = multiplet. The signal abbreviations include H_{Ar} to denote aromatic protons. The ^{13}C NMR signal structure was analyzed by DEPT and is described as follows: + = primary or tertiary C atom (positive signal), − = secondary C atom (negative signal), and C_{quart} = quaternary C atom (no signal). Peak assignments were made on the basis of COSY, HSQC and HMBC experiments. The intensities of the IR spectra recorded as solids are characterized as follows: vs = very strong, 0−10% transmission (T); s = strong, 10−40% T; m = middle, 40−70% T, w = weak, 70−90% T, vw = very weak, 90−100% T. High-resolution mass spectra (HRMS) were obtained by positive matrix-assisted laser desorption/ionization (MALDI) or direct analysis in real time (DART) experiments. Emission spectra of thin films were recorded on glass substrates. Pictures were taken under daylight or illumination at 365 nm. Computational studies were carried out using DFT calculations on Turbomole 6.3.1 or Gaussian 09. Geometry optimizations were performed using the B3LYP functional and def2-TZVP basis set. At this geometry, the absolute energy and FMO energies were assigned by a single-point approach at the B3LYP/6-311++G** level.[20]

Syntheses. Triptycene-2,3-dione (**4**),[28] 2,3-dibromotriptycene (**8**),[29] 1,4-bis((triisopropylsilyl)ethynyl)benzene-2,3-diamine (**5**),[30] 1,4-bis((triisopropylsilyl)ethynyl)naphthalene-2,3-diamine (**6**),[16] 1,4-bis((triisopropylsilyl)ethynyl)anthracene-2,3-diamine (**7**),[17] 1,4-bis((triisopropylsilyl)ethynyl)phenazine (**1b**),[14] 6,11-bis((triisopropylsilyl)ethynyl)benzo[*b*]phenazine (**2b**),[16] and 6,13-bis((triisopropylsilyl)ethynyl)naphtho[2,3-*b*]phenazine (**3b**)[17] were synthesized according to literature procedures.

General Procedure 1 (GP1): Condensation (Method a). A solution of the *o*-quinone compound (1.00 equiv) and the *o*-diamine (1.00 equiv) in a 1:1 mixture of dichloromethane and acetic acid was prepared in a round-bottom flask with a condenser. The solution was heated to reflux for 4 h at 80 °C under stirring. The mixture was cooled to room temperature and carefully diluted with a saturated aqueous solution of sodium hydrogen carbonate (10 mL). The phases were separated, and the organic layer was washed with 10 mL of water followed by 10 mL of brine and then dried over magnesium sulfate. After filtration, the solvent was evaporated, and the crude solid was purified by column chromatography (silicon dioxide; 30 × 4.5; petroleum ether/dichloromethane gradient from 1:0 to 5:1, v/v). To oxidize the formed *N*,*N*′-dihydro species, the solid was dissolved in dichloromethane, and manganese dioxide (15.0 equiv) was added. After 1 h, TLC monitoring showed that no starting material was left. The suspension was filtered, and the solvent was evaporated under reduced pressure. The crude product was purified by column chromatography (silica gel; 25 × 4.5; petroleum ether/dichloromethane 1:0 to 5:1 gradient, v/v).

General Procedure 2 (GP2): Buchwald−Hartwig Cross-Coupling (Method b). A solution of the *o*-dibromide (1.50 equiv) and the *o*-diamine (1.00 equiv) as well as palladium precatalyst **9** (5 mol %) in dry 1,4-dioxane was prepared in an oven-dried microwave vial. The solution was degassed for 30 min by bubbling of argon, and then cesium carbonate (4.00 equiv) was added. The microwave vial was sealed, and the mixture was stirred for 16 h at 120 °C, cooled to room temperature, and diluted with a saturated aqueous solution of ammonium chloride (5 mL). The phases were separated, and the aqueous phase was extracted three times with diethyl ether (20 mL). The combined organic layers were washed three times with brine and dried over magnesium sulfate. The solvent was evaporated, and the crude solid was purified by column chromatography (silicon dioxide; 25 × 4.5; petroleum ether/dichloromethane 1:0 to 5:1 gradient, v/v). To oxidize formed *N*,*N*′-dihydro species, the solid was dissolved in dichloromethane, and manganese dioxide (15.0 equiv) was added. After 1 h, TLC monitoring showed that no starting material was left. The suspension was filtered, and the solvent was evaporated under reduced pressure. The crude product was purified by column chromatography (silica gel; 25 × 4.5; petroleum ether/dichloromethane 1:0 to 5:1 gradient, v/v).

1,4-Bis((triisopropylsilyl)ethynyl)-7,12-dihydro-7,12[1′,2′]-benzeno-5,14-diazapentacene (1a). GP1 was applied to 26.0 mg (91.5 μmol, 1.00 equiv) of 2,3-triptycenequinone and 42.9 mg (91.5 μmol, 1.00 equiv) of 1,4-bis((triisopropylsilyl)ethynyl)benzene-2,3-diamine in 4 mL of dichloromethane and 4 mL of acetic acid. Flash column chromatography yielded fluorescent darkish-yellow crystalline solid **1a**. Yield: 56.2 mg (78.4 μmol, 86%). R_f: 0.28 (petroleum ether/dichloromethane 5:1, v/v). Mp: 122 °C. ^{1}H NMR ($CDCl_3$, 400.33 MHz, 298.1 K): δ 1.25−1.28 (m; 42H; ^{i}Pr-*H*), 5.68 (s; 2H; C_3CH), 7.08−7.12 (m; 4H; CCHCH_{Ar}), 7.49−7.53 (m; 4H; CCH_{Ar}CH), 7.85 (s; 2H; CCCCH_{Ar}), 8.05 (s; 2H; NCCH_{Ar}). ^{13}C NMR (400.33 MHz, $CDCl_3$, 298.2 K): δ 10.7 (+, *C*HCH$_3$), 18.0 (+, CHCH$_3$), 52.7 (+, *C*-7, *C*-12), 99.2 (C_{quart}, CCSi), 103.1 (C_{quart}, *C*CSi), 122.0 (+, *C*-6, *C*-13), 123.30 (+, *C*-8, *C*-11), 123.39 (C_{quart}, *C*-4a, *C*-14a), 125.4 (+, *C*-9, *C*-10), 132.1 (+, *C*-2, *C*-3), 142.17 (C_{quart}, *C*-5a, *C*-13a), 142.22 (C_{quart}, *C*-1, *C*-4), 142.42 (C_{quart}, *C*-7a, *C*-11a), 146.1 (C_{quart}, *C*-6a, *C*-12a). IR (neat): ν [cm^{-1}] 2940 (w), 2889 (vw), 2862 (w), 1460 (w), 1436 (vw), 1426 (w), 1221 (vw), 1147 (vw), 1146 (vw), 1036 (w), 1016 (vw), 995 (w), 882 (w), 846 (w), 791 (w), 735 (w), 675 (w), 660 (w), 628 (w), 621 (w), 587 (w), 537 (vw), 493 (vw), 477 (vw). HRMS (DART FT-ICR) *m*/*z*: [M + H]$^+$ calcd for $C_{48}H_{57}N_2Si_2$ 717.4055; found 717.4046 with correct isotope distribution. Anal. Calcd for $C_{48}H_{56}N_2Si_2$: C, 80.39; H, 7.87; N; 3.91. Found: C, 80.39; H, 8.19; N, 3.68.

5,16-Bis((triisopropylsilyl)ethynyl)-8,13-dihydro-8,13[1′,2′]-benzeno-6,15-diazahexacene (2a). GP1 was carried out with 100 mg (352 μmol, 1.00 equiv) of 2,3-triptycenequinone and 183 mg (352 μmol, 1.00 equiv) of 1,4-bis((triisopropylsilyl)ethynyl)naphthalene-2,3-diamine in 15 mL of dichloromethane and 15 mL of acetic acid. Flash column chromatography yielded fluorescent darkish-red solid **2a**. Yield: 232 mg (302 μmol, 86%). GP2 was applied to 50 mg (121 μmol, 1.50 equiv) of 2,3-dibromotriptycene and 42.0 mg (80.9 μmol,

dx.doi.org/10.1021/jo502564w | J. Org. Chem. 2015, 80, 582−589

1.00 equiv) of 1,4-bis((triisopropylsilyl)ethynyl)naphthalene-2,3-diamine as well as 3.30 mg (4.04 μmol, 5 mol % loading) of palladium precatalyst **9** in 4 mL of dry 1,4-dioxane. Flash column chromatography yielded fluorescent darkish-red amorphous solid **2a**. Yield: 44.1 mg (57.4 μmol, 71%). R_f: 0.30 (petroleum ether/dichloromethane 5:1, v/v)). Mp: 244 °C. ^{1}H NMR ($CDCl_3$, 400.33 MHz, 298.1 K): δ 1.30−1.38 (m; 42H; ^{i}Pr-*H*), 5.67 (s; 2H; C_3CH), 7.10−7.14 (m; 4H; $CCHCH_{Ar}$), 7.50−7.54 (m; 4H; $CCH_{Ar}CH$), 7.59−7.63 (m; 2H; $CCCHCH_{Ar}$), 8.01 (s; 2H; $NCCH_{Ar}$), 8.68−8.73 (m; 2H; $CCCH_{Ar}CH$). ^{13}C NMR (400.33 MHz, $CDCl_3$, 298.2 K): δ 11.8 (+, $CHCH_3$), 19.1 (+, $CHCH_3$), 53.6 (+, *C*-8, *C*-13), 103.2 (C_{quart}, CCSi), 107.5 (C_{quart}, CCSi), 120.7 (C_{quart}, *C*-5, *C*-16), 122.9 (+, *C*-7, *C*-14), 124.3 (+, *C*-9, *C*-12, *C*-3′, *C*-6′), 126.5 (+, *C*-10, *C*-11, *C*-4′, *C*-5′), 127.70 (+, *C*-1, *C*-4), 127.71 (+, *C*-2, *C*-3), 134.9 (C_{quart}, *C*-4a, *C*-16a), 141.2 (C_{quart}, *C*-5a, *C*-15a), 143.1 (C_{quart}, *C*-8a, *C*-12a), 144.4 (C_{quart}, *C*-6a, *C*-14a), 147.0 (C_{quart}, *C*-7a, *C*-13a). IR (neat): ν [cm^{-1}] 2921 (s), 2859 (m), 1733 (w), 1599 (m), 1461 (s), 1379 (m), 1262 (m), 1214 (m), 1016 (m), 882 (m). HRMS (MALDI FT-ICR) *m*/*z*: $[M]^+$ calcd for $C_{52}H_{58}N_2Si_2$ 766.4133; found 766.4135 with correct isotope distribution. Anal. Calcd for $C_{52}H_{58}N_2Si_2$: C, 81.41; H, 7.62; N, 3.65. Found: C, 81.37; H, 7.77; N, 3.59.

6,17-Bis((triisopropylsilyl)ethynyl)-9,14-dihydro-9,14[1′,2′]-benzeno-7,16-diazaheptacene (3a). GP1 was applied to 25 mg (87.9 μmol, 1.00 equiv) of 2,3-triptycenequinone and 50.0 mg (87.9 μmol, 1.00 equiv) of 1,4-bis((triisopropylsilyl)ethynyl)anthracene-2,3-diamine in 15 mL of dichloromethane and 15 mL of acetic acid. Flash column chromatography yielded dark-green solid **3a**. Yield: 67.7 mg (82.8 μmol, 94%). GP2 was carried out with 50 mg (121 μmol, 1.50 equiv) of 2,3-dibromotriptycene and 46.0 mg (80.9 μmol, 1.00 equiv) of 1,4-bis((triisopropylsilyl)ethynyl)anthracene-2,3-diamine as well as 3.30 mg (5 mol % loading) of palladium precatalyst **9** in 4 mL of dry 1,4-dioxane. Flash column chromatography yielded dark-green amorphous solid **3a**. Yield: 33.0 mg (40.4 μmol, 50%). R_f: 0.28 (petroleum ether/dichloromethane 5:1, v/v). Mp: >295 °C (decomp.). ^{1}H NMR ($CDCl_3$, 400.33 MHz, 298.2 K): δ 1.36−1.40 (m; 42H; ^{i}Pr-*H*), 5.65 (s; 2H; C_3CH), 7.11−7.15 (m; 4H; $C_2CHCCHCH_{Ar}$), 7.44−7.47 (m; 2H; $CHCCHCH_{Ar}$), 7.50−7.54 (m; 4H; $C_2CHCCH_{Ar}CH$), 7.95 (s; 2H; $NCCH_{Ar}$), 7.99−8.02 (m; 2H; $CHCCH_{Ar}CH$), 9.38 (s; 2H; $CCCH_{Ar}$). ^{13}C NMR (400.33 MHz, $CDCl_3$, 298.1 K): δ 11.9 (+, $CHCH_3$), 19.2 (+, $CHCH_3$), 53.6 (+, *C*-9, *C*-14), 104.1 (C_{quart}, CCSi), 108.8 (C_{quart}, CCSi), 120.6 (C_{quart}, *C*-6, *C*-17), 122.9 (+, *C*-8, *C*-15), 124.3 (+, *C*-10, *C*-13, *C*-3′, *C*-6′), 126.57 (+, *C*-11, *C*-12, *C*-4′, *C*-5′), 126.64 (+, *C*-2, *C*-3), 126.81 (+, *C*-5, *C*-18), 128.8 (+, *C*-1, *C*-4), 132.4 (C_{quart}, *C*-5a, *C*-17a), 132.9 (C_{quart}, *C*-4a, *C*-18a), 141.0 (C_{quart}, *C*-6a, *C*-16a), 142.9 (C_{quart}, *C*-9a, *C*-13a, *C*-1′, *C*-2′), 144.9 (C_{quart}, *C*-7a, *C*-15a), 147.1 (C_{quart}, *C*-8a, *C*-14a). IR (neat): ν [cm^{-1}] 3068 (vw), 3041 (vw), 2924 (w), 2858 (w), 2719 (vw), 2355 (vw), 2149 (vw), 2118 (vw), 1727 (w), 1620 (vw), 1582 (vw), 1540 (vw), 1503 (vw), 1459 (w), 1424 (w), 1408 (w), 1375 (m), 1275 (w), 1202 (w), 1172 (w), 1138 (w), 1071 (w), 1016 (m), 988 (w), 918 (vw), 881 (m), 797 (vw), 741 (m), 722 (m), 667 (m), 645 (w), 628 (m), 612 (m), 590 (m), 578 (m), 509 (w), 486 (m), 460 (w), 439 (w), 405 (w). HRMS (MALDI FT-ICR) *m*/*z*: $[M]^+$ calcd for $C_{56}H_{60}N_2Si_2$ 816.4290; found 816.4276 with correct isotope distribution. Anal. Calcd for $C_{56}H_{60}N_2Si_2$: C, 82.30; H, 7.40; N, 3.43. Found: C, 82.23; H, 7.79; N, 3.35.

Thin-Film Preparation. For the thin-film preparation, the glass substrates were cleaned two times in an acetone bath under ultrasound for 5 min and then with isopropanol. The surface was finally treated in the plasma furnace (O_2, 0.4 mbar, 100 W, 10 min). Stock solutions of **2a** were prepared with different concentrations (Table S1 in the Supporting Information). The spin-coating velocity was set up at 1500 rpm for 20 s followed by 3000 rpm for 40 s with accelerations shown in Table S1. Too-high concentrations gave inhomogeneous films. The optimal concentration was 5 mg/mL.

Cyclic Voltammetry. The CV experiments were carried out using a platinum working electrode, a platinum/titanium wire auxiliary electrode, a silver wire pseudoreference electrode, a 0.1 M NBu_4PF_6 solution in degassed dry tetrahydrofuran, and ferrocene/ferrocenium as the reference redox system and internal standard (−5.1 eV[19]). To determine the first reduction potentials ($E^{(0/-)}$) of **1a**−**3a** and the first oxidation potential of ferrocene, the half-wave potentials were used[19] (see the Supporting Information).

OLED Preparation. OLEDs were prepared as follows: Glass substrates covered by a 160 nm layer of ITO ($R_Y \approx 10\ \Omega/Y$) were subsequently cleaned in acetone and isopropanol under sonication for 15 min and treated by O_2 plasma for 5 min. Then PEDOT:PSS solution (Heraeus VPAi 4083, water-diluted 1:1) was filtered with a 0.45 μm PVDF filter, spin-coated under ambient conditions, and annealed on a hot plate at 120 °C for 20 min. The spin-coating parameters were ω = 3000 rpm, *a* = 1000 rpm/s, and *t* = 30 s, resulting in a layer thickness of about 30 nm. Afterward, the samples were transferred to a glovebox with a nitrogen atmosphere. **2a** was dissolved in toluene with a concentration of 15 g/L and filtered with a 0.2 μm PTFE filter before spin-coating. The spin-coating parameters were ω = 2000 rpm, *a* = 1000 rpm/s, and *t* = 60 s, delivering a layer thickness of approximately 60 nm. Finally, the samples were annealed on a hot plate at 115 °C for 15 min and subsequently transferred to a vacuum system with a base pressure of 1×10^{-7} mbar. As the cathode layer, a 10 nm layer of Ca followed by a 100 nm layer of Al was evaporated. All of the OLEDs were encapsulated by barrier foil, acquired from 3M, and subsequently characterized in a BoTest LIV Functionality Test System. In order to check the reproducibility of our OLEDs, we prepared three equivalent devices. In Table S2 in the Supporting Information are listed average values as well as corresponding standard deviations of the turn-on voltage, luminance at 6.5 V, and maximum current efficiency. As can be seen, the variations between different devices were low, with standard deviations of around 5% of the respective average values.

■ ASSOCIATED CONTENT

Supporting Information

Thin-film preparation parameters and photograph of a thin film, full-scale PL spectra, cyclic voltammograms, FMO computational results, Cartesian coordinates of computationally studied molecules, a photograph of an OLED pixel and OLED parameters, copies of NMR spectra (^{1}H and ^{13}C), and crystallographic data (CIF). This material is available free of charge via the Internet at http://pubs.acs.org.

■ AUTHOR INFORMATION

Corresponding Author

*E-mail: Uwe.bunz@oci.uni-heidelberg.de.

Notes

The authors declare no competing financial interest.

■ ACKNOWLEDGMENTS

P.B. thanks the Fonds der Chemischen Industrie for a Kekulé Scholarship. J.U.E. thanks the Deutsche Telekom-Stiftung for a scholarship. We thank the Deutsche Forschungsgemeinschaft (DFG BU 771/7-1) and HeiKa (Heidelberg Karlsruhe Research Partnership) for generous grants.

■ REFERENCES

(1) Anthony, J. E. *Angew. Chem., Int. Ed.* **2008**, *47*, 452.
(2) Anthony, J. E. *Chem. Rev.* **2006**, *106*, 5028.
(3) Odom, S. A.; Parkin, S. R.; Anthony, J. E. *Org. Lett.* **2003**, *5*, 4245.
(4) Wolak, M. A.; Melinger, J. S.; Lane, P. A.; Palilis, L. C.; Landis, C. A.; Delcamp, J.; Anthony, J. E.; Kafafi, Z. H. *J. Phys. Chem. B* **2006**, *110*, 7928.
(5) Richards, G. J.; Hill, J. P.; Mori, T.; Ariga, K. *Org. Biomol. Chem.* **2011**, *9*, 5005.
(6) Chong, J. H.; MacLachlan, M. J. *Chem. Soc. Rev.* **2009**, *38*, 3301.
(7) Kohl, B.; Rominger, F.; Mastalerz, M. *Org. Lett.* **2014**, *16*, 704.
(8) Swager, T. M. *Acc. Chem. Res.* **2008**, *41*, 1181.
(9) Chong, J. H.; MacLachlan, M. J. *J. Org. Chem.* **2007**, *72*, 8683.

(10) Yang, J.-S.; Yan, J.-L. *Chem. Commun.* **2008**, 1501.
(11) Chou, H.-H.; Shih, H.-H.; Cheng, C.-H. *J. Mater. Chem.* **2010**, *20*, 798.
(12) Chen, J. P.; Okamura, Y. Organic light-emitting device using iptycene derivatives. U.S. Patent 6,962,758, 2004.
(13) Salbeck, J.; Becker, H.; Kreuder, W.; Weinfurtner, K. H. Triptycene derivatives and their use for opto-electronics applications, in particular as electroluminescent materials. U.S. Patent 6,509,110, 1999.
(14) Bryant, J. J.; Zhang, Y.; Lindner, B. D.; Davey, E. A.; Appleton, A. L.; Qian, X.; Bunz, U. H. F. *J. Org. Chem.* **2012**, *77*, 7479.
(15) Engelhart, J. U.; Lindner, B. D.; Tverskoy, O.; Rominger, F.; Bunz, U. H. F. *Chem.—Eur. J.* **2013**, *19*, 15089.
(16) Miao, S.; Brombosz, S. M.; Schleyer, P. v. R.; Wu, J. I.; Barlow, S.; Marder, S. R.; Hardcastle, K. I.; Bunz, U. H. F. *J. Am. Chem. Soc.* **2008**, *130*, 7339.
(17) Appleton, A. L.; Brombosz, S. M.; Barlow, S.; Sears, J. S.; Bredas, J.-L.; Marder, S. R.; Bunz, U. H. F. *Nat. Commun.* **2010**, *1*, No. 91.
(18) Lindner, B. D.; Engelhart, J. U.; Märken, M.; Tverskoy, O.; Appleton, A. L.; Rominger, F.; Hardcastle, K. I.; Enders, M.; Bunz, U. H. F. *Chem.—Eur. J.* **2012**, *18*, 4627.
(19) Cardona, C. M.; Li, W.; Kaifer, A. E.; Stockdale, D.; Bazan, G. C. *Adv. Mater.* **2011**, *23*, 2367.
(20) Frisch, M. J.; Trucks, G. W.; Schlegel, H. B.; Scuseria, G. E.; Robb, M. A.; Cheeseman, J. R.; Scalmani, G.; Barone, V.; Mennucci, B.; Petersson, G. A.; Nakatsuji, H.; Caricato, M.; Li, X.; Hratchian, H. P.; Izmaylov, A. F.; Bloino, J.; Zheng, G.; Sonnenberg, J. L.; Hada, M.; Ehara, M.; Toyota, K.; Fukuda, R.; Hasegawa, J.; Ishida, M.; Nakajima, T.; Honda, Y.; Kitao, O.; Nakai, H.; Vreven, T.; Montgomery, J. A., Jr.; Peralta, J. E.; Ogliaro, F.; Bearpark, M. J.; Heyd, J.; Brothers, E. N.; Kudin, K. N.; Staroverov, V. N.; Kobayashi, R.; Normand, J.; Raghavachari, K.; Rendell, A. P.; Burant, J. C.; Iyengar, S. S.; Tomasi, J.; Cossi, M.; Rega, N.; Millam, N. J.; Klene, M.; Knox, J. E.; Cross, J. B.; Bakken, V.; Adamo, C.; Jaramillo, J.; Gomperts, R.; Stratmann, R. E.; Yazyev, O.; Austin, A. J.; Cammi, R.; Pomelli, C.; Ochterski, J. W.; Martin, R. L.; Morokuma, K.; Zakrzewski, V. G.; Voth, G. A.; Salvador, P.; Dannenberg, J. J.; Dapprich, S.; Daniels, A. D.; Farkas, Ö.; Foresman, J. B.; Ortiz, J. V.; Cioslowski, J.; Fox, D. J. *Gaussian 09*; Gaussian, Inc.: Wallingford, CT, 2009.
(21) TURBOMOLE V6.3.1 2011, a development of University of Karlsruhe and Forschungszentrum Karlsruhe GmbH, 1989−2007, TURBOMOLE GmbH, since 2007; available from http://www.turbomole.com.
(22) Lindner, B. D.; Zhang, Y.; Höfle, S.; Berger, N.; Teusch, C.; Jesper, M.; Hardcastle, K. I.; Qian, X.; Lemmer, U.; Colsmann, A.; Bunz, U. H. F.; Hamburger, M. *J. Mater. Chem. C* **2013**, *1*, 5718.
(23) Winkler, M.; Houk, K. N. *J. Am. Chem. Soc.* **2007**, *129*, 1805.
(24) Lindner, B. D.; Engelhart, J. U.; Tverskoy, O.; Appleton, A. L.; Rominger, F.; Peters, A.; Himmel, H.-J.; Bunz, U. H. F. *Angew. Chem., Int. Ed.* **2011**, *50*, 8588.
(25) Shirota, Y.; Kageyama, H. *Chem. Rev.* **2007**, *107*, 953.
(26) Yang, J.-S.; Swager, T. M. *J. Am. Chem. Soc.* **1998**, *120*, 11864.
(27) Gottlieb, H. E.; Kotlyar, V.; Nudelman, A. *J. Org. Chem.* **1997**, *62*, 7512.
(28) Zhao, J.-M.; Lu, H.-Y.; Cao, J.; Jiang, Y.; Chen, C.-F. *Tetrahedron Lett.* **2009**, *50*, 219.
(29) Lee, C.-H.; Guo, J.; Chen, L. X.; Mandal, B. K. *J. Org. Chem.* **2008**, *73*, 8219.
(30) Lindner, B. D.; Coombs, B. A.; Schaffroth, M.; Engelhart, J. U.; Tverskoy, O.; Rominger, F.; Hamburger, M.; Bunz, U. H. F. *Org. Lett.* **2013**, *15*, 666.